RSC Advances

ROYAL SOCIETY OF CHEMISTRY

www.rsc.org/advances

RSC Advances

Paper

Edge Functionalization and Doping Effects on Stability, Electronic and Magnetic Properties of Silicene Nanoribbons

Received 00th January 20xx,
Accepted 00th January 20xx

DOI: 10.1039/x0xx00000x

www.rsc.org/

S. M. Aghaei,[a] M. M. Monshi,[a] I. Torres,[a] and I. Calizo[a,b]

Through density functional theory calculations the impact of edge functionalization on the structural stabilities, electronic and magnetic properties of silicene nanoribbons (SiNRs) are investigated. –H, –F, –Cl, –Br, and –I edge functionalization of armchair, zigzag, Klein, reconstructed Klein, reconstructed pentagon-heptagon edge types, and their combinations are examined. It is found for the first time that trifluorinated Klein edge SiNR is the most stable edge structure among all edge structures of SiNRs. Furthermore, the stability of trihydrogenated Klein edge SiNR, which is periodically replaced by a dihydrogenated zigzag edge, approaches that of dihydrogenated armchair edge SiNR as the most stable hydrogenated SiNR. It is revealed that asymmetry in edge functionalization or combining different edge types can transform symmetric edge functionalized zigzag SiNRs from antiferromagnetic semiconductors to various magnetic states, such as bipolar spin gapless semiconductors (SGS), ferromagnetic metals and semiconductors, and antiferromagnetic metals. Furthermore, the effects of N or B doping on the stability, electronic and magnetic properties of hydrogenated and fluorinated SiNRs are studied. It is discovered that the mono-fluorinated armchair SiNR shows a SGS behavior with 100% spin polarized currents around the Fermi level, when the Si edge atom is substituted by N or B atom. The remarkable SGS and half-metal characters, and ferromagnetic metals are also observed in N- or B- doped asymmetric edge functionalized zigzag SiNRs, fully functionalized Klein edge SiNRs, and combinations of zigzag SiNRs with reconstructed Klein edge SiNRs. These results encourage further experimental investigations in the development of SiNRs-based nanoelectronics with spin tuning.

I Introduction

Graphene has garnered great attention due to its potential applications.[1,2] Despite its many benefits, challenges like large area growth of graphene, processing difficulties, incompatibility with existing silicon-based devices, and toxicity hamper the advancement of graphene-based electronic devices. Silicon, the backbone of current electronic devices, has many similarities with carbon. Inspired by the success of graphene, other 2D honeycomb lattice materials such as silicene, have attracted enormous interest.[3-7] Silicene, the 2D counterpart of silicon, was first reported by Takeda and Shiraishi in 1994,[8] and its name coined by Guzmán-Verri and Voon in 2007.[9] It was synthesized on various substrates such as Ag (111),[10-12] Ir (111),[13] ZrB_2 (0001),[14] and ZrC (111)[15] in order to increase silicene's stability. Silicene and graphene have a similar band structure. Theoretically, the conduction and valence band have linear crossing at the Fermi level (E_F), creating Dirac cones.[16,17] Thus, electrons propagate through silicene behaving like massless fermions with a large Fermi velocity ranging from 10^5 to 10^6 ms^{-1}.[18] Differing from a flat graphene sheet, a stable silicene sheet is low buckled with a buckling distance of 0.44 Å,[9,19,20] reflecting the tendency of silicon atoms to adopt a mixture of sp^2 + sp^3 hybridization over sp^2 hybridization in silicene. The buckled structure of silicene produces an additional intrinsic Rashba spin-orbit coupling (SOC) which is non-existent in graphene, playing a significant role in spin transport.[21] It is found that SOC induces a band gap of 23.9 meV at the K-point which is much greater than that of graphene.[22] In order to retain the buckled structure of silicene and its freestanding electronic properties, various substrates like BN, SiC, GaS, and graphene, which have weak Van der Waals interactions with silicene, have been recently studied.[23-26]

Silicene nanoribbons (SiNRs) is one method to open a band gap in a silicene sheet [19,25] and have already been grown on different substrates such as Ag (110) and Au (110).[27-30] Similar to graphene,[31] armchair and zigzag/Klein edges can be formed by cutting the silicene honeycomb lattice along $<1\bar{1}10>$ and $<2\bar{1}\bar{1}0>$ directions, respectively. Mixtures of different edge types give rise to intermediate orientations, so-called chiral edges. Recently, several studies have probed the electronic and magnetic properties of SiNRs.[25,32-39] Dávila *et al.*[33] demonstrated that hydrogen can alter the geometry and electronic properties of isolated and self-assembled SiNRs grown on Ag (110) substrate. On the basis of density functional

[a] Quantum Electronic Structures Technology Lab, Department of Electrical and Computer Engineering, Florida International University, Miami, Florida 33174, United States
[b] Department of Mechanical and Materials Engineering, Florida International University, Miami, Florida 33174, United States

Electronic Supplementary Information (ESI) available: [details of any supplementary information available should be included here]. See DOI: 10.1039/x0xx00000x

theory calculations (DFT), Ding *et al.*[25] studied completely hydrogenated armchair SiNR (ASiNRs) and zigzag SiNRs (ZSiNRs). They found that the band gap of ASiNRs decreases with increasing ribbon width oscillating with a period of three. Moreover, they revealed that ZSiNRs exhibit antiferromagnetic (AFM) semiconducting behavior. Like zigzag edge graphene nanoribbons (GNRs) in which having ferromagnetic (FM) semiconducting behavior is desirable for spintronics applications,[40,41] it is important to discover approaches that induce ferromagnetism in the ZSiNRs while retaining its semiconducting behavior. It was proven that edge states can dramatically modify the electronic and magnetic properties of GNRs.[42-49] Edge functionalization is an attractive method to tailor the properties of SiNRs and can convert the system into spin-gapless semiconductors (SGS), intrinsic half-metals, or ferromagnetic metals.[50-53]

Recently, the effects of chemical doping on the electronic and magnetic properties of SiNRs have been investigated.[54-59] Special attention was paid to 2p elements such as B, N, and P atoms due to their chemical propinquity to silicon.[60] A spectacular SGS character with 100% spin polarized currents around the Fermi level was observed in ZSiNRs doped with N atom at the edge.[54,55] While ASiNRs experience a semiconductor-metal transition when doped with B or N atoms at the edges.[55] When a B-N pair is introduced into SiNRs, the ASiNRs remain semiconductor, while for the ZSiNRs, it causes a transition from nonmagnetic (NM) to spin-polarized state and SGS.[56] Fang *et al.*[50] found that the ZSiNRs doped with N or P atoms can become half-metal under a perpendicular electric field. Interestingly, a bipolar magnetic semiconducting behavior was found in asymmetric hydrogenated ZSiNRs, which can be converted to half-metal by B or P doping.[51]

However, to the best of our knowledge, no in depth study to this point has comprehensively explored the full range of SiNRs edge types with different functional addends. In this paper, we employ first-principles method based on DFT to investigate the effects of edge hydrogenation (-H) and halogenation (-F, -Cl, -Br, and -I) on the geometry, stability, electronic and magnetic properties of different SiNRs edge types. Additionally, the impacts of N or B atoms on the stability, electronic and magnetic properties of different SiNRs functionalized with hydrogen atom or fluorine atom are explored. Our results serve as a useful guide for experimental synthesis groups and theoretical studies in tuning the electronic and magnetic properties of stable SiNRs.

II Computational Methods

Calculations are performed using first-principles method based on self-consistent DFT combined with nonequilibrium Green's function (NEGF), carried out using ATOMISTIX TOOLKIT (ATK).[61-63] The Perdew-Burke-Ernzerhof (PBE) parameterized Generalized Gradient Approximation (GGA) exchange correlation with a double-ζ polarized basis set and a density mesh cut off of 150 Rydberg are utilized to solve Kohn-Sham equation and expand electronic density. All the structures are treated with periodic boundary conditions. In order to suppress any interactions between the structure and its periodic image, a vacuum space of 15 Å is considered in each side of the supercell. In addition, the electronic temperature of the structures is kept constant at 300 °K. Prior to the calculations, all the atomic positions and lattice constants are allowed to relax until the force and stress on them become less than 0.05 eV/Å and 0.001 eV/ Å^3, respectively. A *k* mesh of 1×1×21 is used for sampling of the Brillouin zone during the optimization. In order to extract accurate electronic and magnetic properties for the structures, the *k* mesh is increased to 1×1×121.

III Results and Discussions

As reported previously for graphene sheet,[31] it is predicted that cutting silicene sheets along the $<1\bar{1}10>$ and $<2\bar{1}\bar{1}0>$ directions results in armchair and parallel zigzag/Klein edges, respectively, as shown in **Fig. 1.** Furthermore, silicene edges are expected to undergo reconstruction of Klein edges in order to enhance their stability. All intermediate orientations, which are made by altering parts of edge orientations or mixing different edge types together, are called chiral edges. In order to distinguish the various functionalized edge configurations of SiNRs, a nomenclature similar to the Ref. 42 is used as follows: *a*: armchair, *z*: zigzag, *k*: Klein, and *rk*: reconstructed Klein. Additionally, the subscripts denote the number of hydrogen or halogen atoms attached to each silicon edge atom along the periodic direction in the supercell, and the hyphen between numbers in the subscripts separate the number of hydrogen or halogen atoms attached to one edge from another. In this paper, a detailed theoretical report is given on the impacts of edge functionalization on the electronic and magnetic properties of ASiNR, ZSiNR, and all chiral edges with a width of 7. For this reason, X atoms (X = H, F, Cl, Br, and I) with different densities are attached to the silicon edge atoms. Finally, the influence of N or B doping on the electronic and magnetic properties of SiNRs are studied.

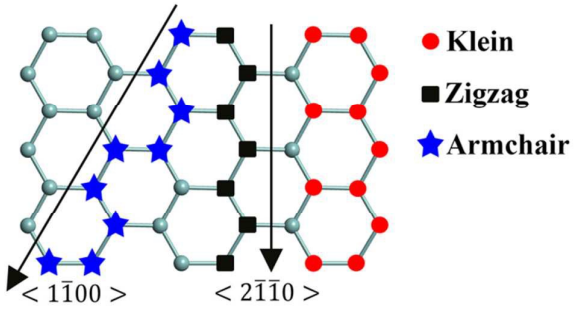

Fig. 1 Cutting a silicene sheet along the $<1\bar{1}10>$ and $<2\bar{1}\bar{1}0>$ directions create armchair (blue solid stars) and zigzag (black solid squares) or Klein (red solid circles) edges, respectively.

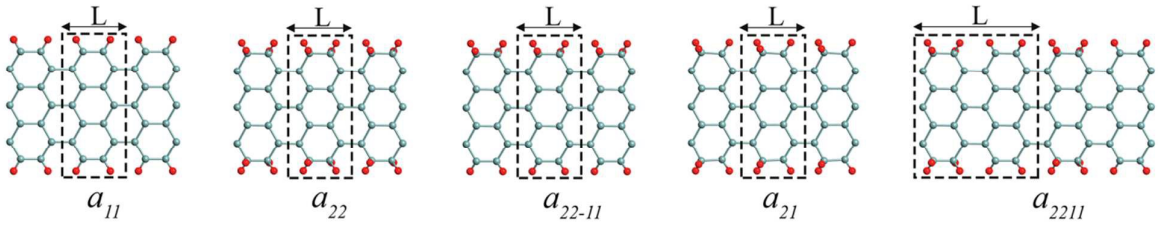

Fig. 2 Schematic structural models of the different edge functionalized 7-ASiNRs. L is the periodic length of the structure. The primitive supercell is marked by a dashed black box. The cyan and red balls represent Si and functional addends (H, F, Cl, Br, and I), respectively.

3.1 Armchair Silicene Nanoribbons

Three common forms of edge hydrogenation and halogenation are studied: mono-atom on both edges (a_{11}), di-atoms on both edges (a_{22}), and di-atoms on one edge and mono-atom on the other edge ($a_{22\text{-}11}$), as shown in **Fig. 2.** In addition, we considered the a_{21} structure in which silicon atoms are periodically attached to mono-hydrogen (-halogen) and di-hydrogen (-halogen) and a_{2211} structure which is a mix of a_{22} and a_{11} structures. The stability of edge functionalized ASiNRs can be determined by calculating formation energies. If the nanoribbon segment in one supercell contains n_{Si} silicon atoms and n_{X2} hydrogen or halogen atoms, the average edge formation energy of functionalized SiNRs is expressed as

$$E_{edge} = \frac{1}{2L}\left(E_{ribbon} - n_{Si} \times E_{Si} - n_X \times E_{X_2}/2\right)$$

where E_{ribbon} represents the total energy of the functionalized SiNR in a supercell. E_{Si} and E_{X2} are the total energy of free Si and isolated hydrogen or halogen molecule, respectively. n_{Si} and n_X are the number of Si atoms in the supercell and the number of hydrogen or halogen atoms attached to the edges, respectively. L is the periodic length of the nanoribbon and 2 accounts for two edges of the nanoribbon. The negative values of E_{edge} correspond to an exothermic process in perfect vacuum conditions around freestanding SiNRs. The edge formation energies, band gap energy, and magnetic edge states of various ASiNRs configurations are listed in **Table S1.** The ASiNR with bare edges is unstable (+ 0.33 eV/Å). The precise edge functionalizing of SiNR is one way to increase its stability. Among all configurations of hydrogenated ASiNR, a_{22} (– 0.13 eV/Å) is the most stable. The stability of ASiNRs has even been increased by halogenation, for instance, the value of formation energy of a_{22} when functionalized with fluorine atoms has decreased to – 2.48 eV/Å, 19 times more stable than hydrogenated a_{22}. The stability of halogenated ASiNRs decreases as the atomic number of the halogen atoms increases. However, they are still much more stable than hydrogenated ASiNRs. To consolidate the obtained results, the stability of the a_{22} functionalized with a combination of hydrogen and fluorine atoms is investigated. **Fig. 3** shows the edge formation energy changes of edge functionalized a_{22} for different combinations of H and F atoms on the edges. It is clear that the edge formation energy decreases with increased F atoms attached to Si edge atoms confirming our findings that the halogenation would increase the stability of the structures.

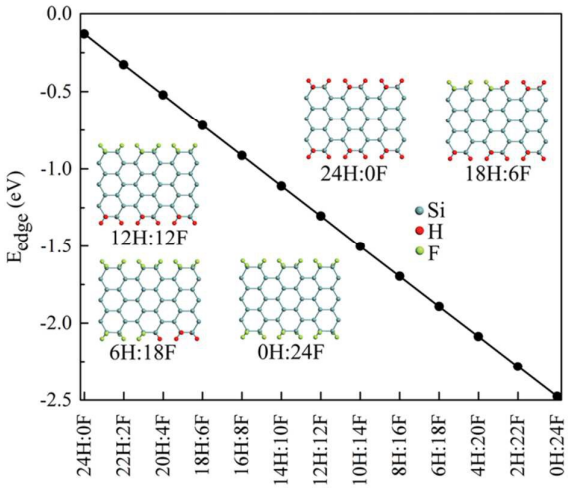

Fig. 3 Edge formation energy of a_{22} for different ratios of H:F attached to Si edge atoms. Insets show schematic models of functionalized a_{22} with different H:F ratios. The cyan, red, green balls represent Si, H and F atoms, respectively.

In order to consider the influence of experimental conditions, temperature and gas pressure, on the stability of functionalized SiNRs, the calculated edge formation energy can be compared to the chemical potential (μ_{X2}) of the hydrogen or halogen molecule. For this purpose, we calculate the edge free energy γ_X(T,P) using the following formula[64,65]

$$\gamma_X(T,p) = E_{edge} - \frac{1}{2} \times \rho_X \times (\mu_{X_2}(T,p) - E_{X_2})$$

Here, $\rho_x = n_x/2L$ is the hydrogen or halogen edge density. The hydrogen or halogen chemical potential μ_{X2} depends on the experiment's temperature and gas pressure according to the following formula[64,65]

$$\mu_{X_2}(T,p) = E_{X_2} + \mu^o{}_{X_2}(T,p)$$

The zero reference state of μ_{X2} *(T,P)* is chosen to be the total energy of an isolated hydrogen or halogen molecule E_{X2} *at* T = 0*, i.e.,* μ_{X2} *(0,p)* = $E_{X2} \equiv 0$. With respect to this zero, the temperature and pressure dependence contribution to the chemical potential is then given by[64,65]

$$\mu^o_{X_2}(T,p) = H^o(T) - H^o(0) - TS^o(T) + k_B T \ln\left(p/p^o\right)$$

Here, $H^o(S^o)$ is the enthalpy (entropy) of hydrogen or halogen molecule at the pressure p^o = 1 bar, which is obtained from Ref. 66. It is important to define the thermodynamic limits of hydrogen's or halogen's chemical potential. The upper limits are defined by the chemical potential at which hydrogen or halogen molecule is formed, which is equal to the total energy of an isolated molecule at T = 0 K.

$$\max[\mu_{X_2}(T,p)] = E_{X_2}$$

The lower limits are chosen for those hydrogen or halogen potentials that are accessible experimentally at very high temperature (900K).

$$\min[\mu_{X_2}(900,p)] = E_{X_2} + \mu^o_{X_2}(900,p)$$

Using Ref. 66, the value of the second term for hydrogen and fluorine molecules at a pressure of 1 bar is –1.52 eV and –2.24 eV, respectively. Therefore, the allowed range of the chemical potential, considering E_{X2} as zero reference, for the hydrogen molecule is

$$-1.52 \prec \mu_{H_2}(T,p) - E_{H_2} \prec 0$$

and for the fluorine molecule is

$$-2.24 \prec \mu_{F_2}(T,p) - E_{F_2} \prec 0$$

The variations of edge free energy with respect to chemical potential of, for example, the H_2 molecule, using E_{H2} as zero reference, for different ASiNRs configurations are calculated, as shown in **Fig. 4.** Under H-poor conditions with $\mu_{H2} < -1.419$ eV, the a_{11} is favorable for ASiNRs. While, when $\mu_{H2} \geq -1.419$ eV, the a_{22} becomes more stable than other configurations. Interestingly, under ambient conditions, i.e., 300 K and 5×10^{-7} bar ($\mu_{H2} = -0.694$ eV), a_{22} has minimum energy. It should be added that for fluorine, a_{22} edge structure is always the most stable structure. **(See Fig. S1(a)).**

Fig. 5(a) shows the variations of band gap of hydrogenated a_{11}, a_{22}, and $a_{22\text{-}11}$ with respect to the ribbon width (N). Similar to the trend of the band gap energy in the most widely studied case, hydrogenated a_{11}, the band gap of all configurations oscillate with 3N periodicity.[19,32,55] They can be classified into three branches with width 3N − 1, 3N, and 3N + 1, where N is an integer. Similar to armchair GNRs, the three branches with decaying profiles in band gaps originate from the quantum size effect which has been already proved in the literature.[67,68] Interestingly, comparing the variations of band gap of a_{22} and $a_{22\text{-}11}$ with a_{11}, a shift is visible. The values of band gap for a_{11}, $a_{22\text{-}11}$, *and* a_{22} with width of N, N + 1, and N + 2 are almost equal. A Si atom shares four valence electrons (Ne $2s^2 2p^2$) in the ribbon. Since the contributions of s orbitals are too small near the Fermi level, only p_z orbitals should be considered. For a_{11}, each Si atom at the edge is connected to two Si atoms and one H by sp^2 hybridization; therefore, p_z orbitals of all the edge and inner Si atoms contribute to the band gap. However, for a_{22}, Si atoms at the edge are bonded to two Si atoms and two H atoms by sp^3 hybridization. Therefore, p_z orbitals are not available anymore. This means that dihydrogenation of one armchair edge of the ribbon decreases the ribbon width (N) of a_{11} by one due to the reduction of the sp^2 hybridization of the edge silicon atom. For example, an a_{22} with a width of N + 2 can be modeled as a combination of two edges with sp^3 hybridization that makes a large band gap due to strong quantum confinement and an internal ASiNR with sp^2 hybridization, with a width of N, with a much smaller band gap that is equal to value of band gap of a_{11}. The band gap of this combination is defined by the latter which is equal to the band gap of a_{11}. These findings have previously been observed for graphene.[36,49,69]

As can be seen in **Table S1,** the nanoribbons functionalized with hydrogen have comparable edge formation energies for $a_{22\text{-}11}$ and a_{2211} configurations (− 0.02 eV), however, these configurations have different energy band gaps (0.446 eV and 0.308 eV, respectively). The primitive supercell of $a_{22\text{-}11}$ includes 14 Si atoms and 6 H atoms, while there are 28 Si atoms and 12 H atoms in the primitive supercell of a_{2211}, as shown in **Fig. 2**. If the supercell size of $a_{22\text{-}11}$ is doubled, the number of Si and H atoms in the new supercell of $a_{22\text{-}11}$ *and* the primitive supercell of a_{2211} would be equal. The edge formation energies of both nanoribbons would be almost equal since there are 4 dihydrogenated Si edge atoms and 4 mono-hydrogenated Si edge atoms in both supercells. However, as mentioned before, the band gap would be defined by the size of the quantum confinement effect which strongly depends on the width of the nanoribbon. Also, it was revealed that the dihydrogenation would decrease the effective ribbon width by one. As a result, while, the two structures have the same edge formation energies, their energy band gap values are different because of different the quantum confinement strengths.

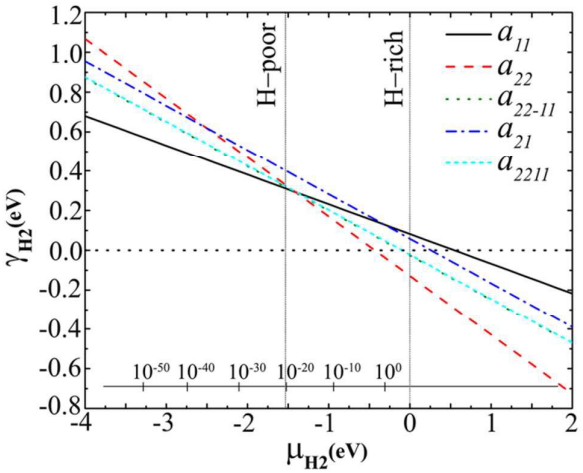

Fig. 4 Edge free energy γ_{H2} of hydrogenated edge ASiNRs studied as a function of hydrogen chemical potential μ_{H2}, using E_{H2} as the zero reference. The allowed range for hydrogen chemical potential is indicated by vertical dotted lines. The bottom inset axis represents the pressure (bar), of molecular H_2 corresponding to μ_{H2} when T = 300 K.

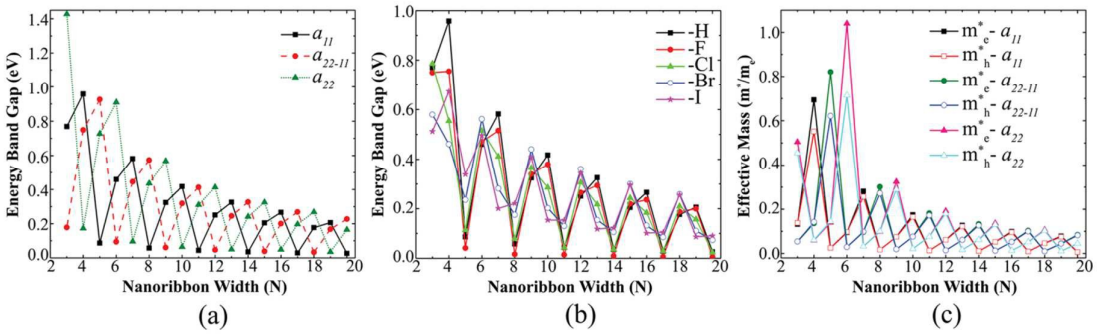

Fig. 5 (a) The energy band gap changes *versus* nanoribbon width for hydrogenated a_{11}, $a_{22\text{-}11}$, and a_{22} (b) The energy band gap variations of hydrogenated and halogenated a_{11} with nanoribbon width (c) effective electron (m_e^*) and hole (m_h^*) mass changes of hydrogenated a_{11}, $a_{22\text{-}11}$, *and* a_{22} with respect to nanoribbon width at the Γ-point.

Furthermore, the bad gap changes of hydrogenated and halogenated a_{11} with nanoribbon width are compared in **Fig. 5(b).** It is clear that halogenation results in a reduction of band gap values. However, it maintains the oscillatory behavior which is found in the hydrogenated case. In hydrogenated ASiNR, the Si-H bond is covalent. The electrons of hydrogen occupy the empty lowest conduction band of silicene, leaving the Si-Si bonds unchanged.[70] Nonetheless, in the halogenated ASiNR, the Si-X (X = F, Cl, Br, and I) bond shows ionic characteristics. The values of Pauling electronegativity of X are 3.98, 3.16, 2.96, and 2.66, respectively, much larger than that of silicon which is 1.90.[71] The van der Waals radiuses for hydrogen and X atoms are 1.20, 1.47, 1.75, 1.85, and 1.98 Å, respectively.[71] In a perfect ASiNR, the Si-Si bond length (2.28 Å) is almost twice that of hydrogen van der Waals radius, suggesting that steric hindrance can be ignored in pristine ASiNRs. However, steric hindrance should be accounted for in halogenated ASiNRs. The steric hindrance effect becomes noticeably stronger with increasing atomic number of halogens due to increasing of van der Waals radiuses. As a result, the ionic characteristic of the Si-X bond and interaction between Si and functional atoms make the Si-Si bond weaker. They also reduce the electron population in the bonding orbitals of Si, bonding-antibonding splitting, and consequently the energy band gap of ASiNRs.[49,72]

Variations of electron and hole effective masses of hydrogenated a_{11}, a_{22}, and $a_{22\text{-}11}$ with respect to nanoribbon width are also calculated, as plotted in **Fig. 5(c)**. Similar to the band gap's trend, effective masses of hydrogenated a_{11} oscillate with 3N periodicity and shift when one edge is dihydrogenated. The larger band gaps associated with larger carrier effective masses and thus lower mobilities at the band edges, suggesting that functionalization is an effective approach to control the transport properties of SiNRs. The results are in good agreement with previous observations for graphene.[49]

The spin-polarized calculations show that all a_{11}, a_{22}, and a_{2211} configurations are NM, exceptionally, unlike other configurations of ASiNRs, the hydrogenated or halogenated a_{21} structure shows metallic behavior. The spin-polarized calculations of hydrogenated a_{21} show that they are FM semiconductors with a direct band gap of 0.888 eV for spin-up channel and indirect band gap of 0.697 eV for spin-down channel, as shown in **Fig. 6.** The energy difference between FM and AFM states (ΔE_{FM-AFM}) is –86.55 meV. However, the fluorinated a_{21} is an AFM metal considering spin polarization.

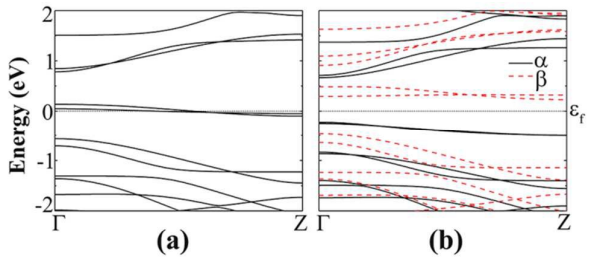

Fig. 6 Band structures of hydrogenated a_{21} in the (a) NM and (b) FM states. The Fermi energy is set at zero. α (black solid line) and β (red dashed line) represent spin-up and spin-down bands, respectively.

3.2 Zigzag / Klein edge Silicene Nanoribbons

The $<2\bar{1}\bar{1}0>$ orientation is much more complicated than $<1\bar{1}\bar{1}0>$. As can be seen in **Fig. 1**, there are two primary parallel possibilities for SiNRs in the $<2\bar{1}\bar{1}0>$ direction, calling the zigzag edge and the Klein edge. The bare ZSiNR is highly unstable (+ 0.38 eV/Å). Various forms of edge functionalization with hydrogen and halogens are considered to improve the stability of ZSiNRs. In addition to well-known structures of z_1, z_2, and $z_{2\text{-}1}$, some other possible forms of edge functionalization of ZSiNRs are considered, including z_{21}, z_{211}, and z_{221}, as seen in **Fig. 7.**

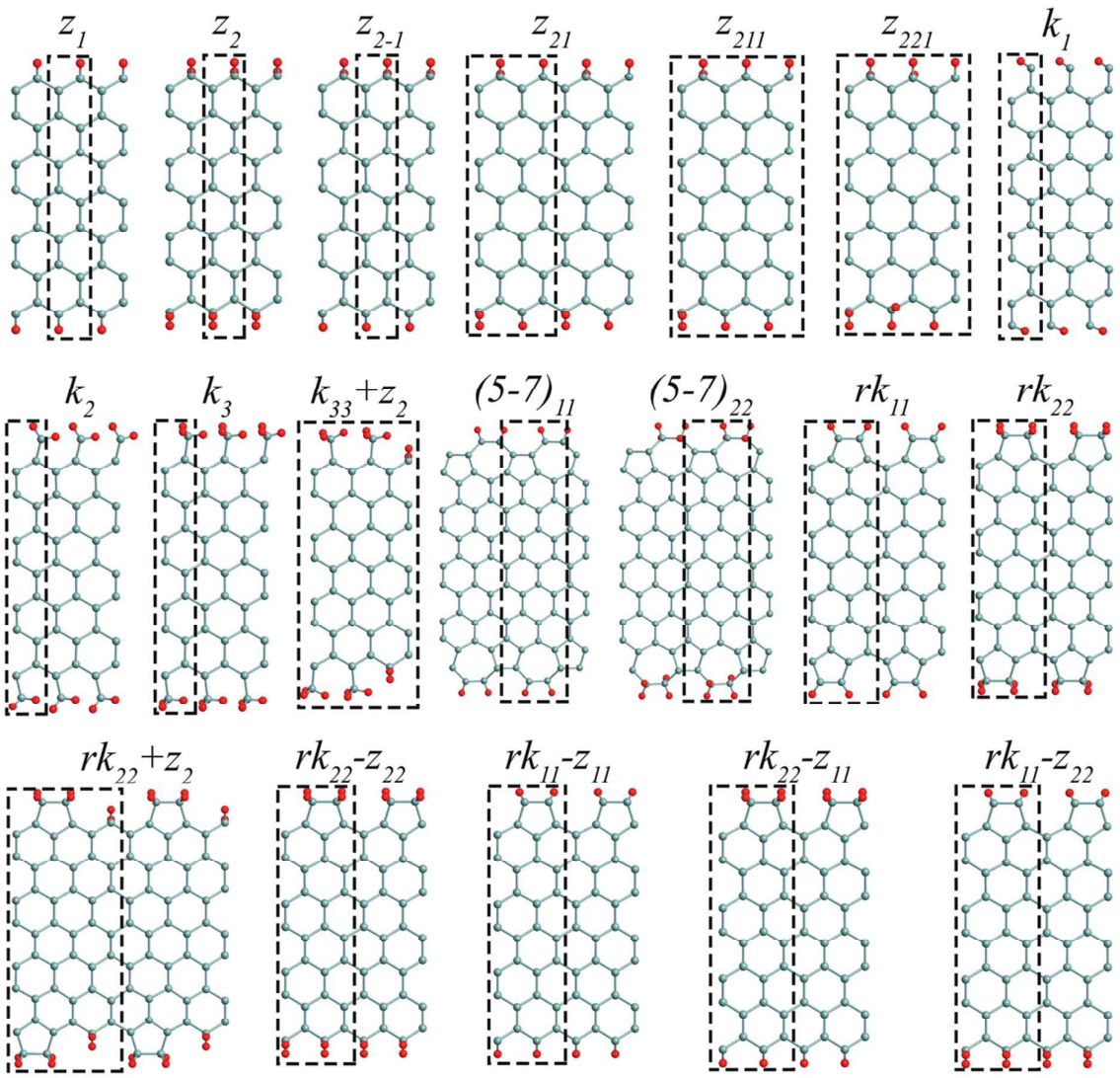

Fig. 7 Different edge structures of functionalized SiNRs along $<2\bar{1}\bar{1}0>$ direction. L is the periodic length of the structure. The primitive supercell is marked by a dashed black box. The cyan and red balls represent Si and functional addends (H, F, Cl, Br, and I), respectively.

The edge formation energies, band gap energies, and magnetic edge states of various ZSiNRs are listed in **Table S2.** Among all possible edge hydrogenation forms of ZSiNRs, the z_2 (− 0.009 eV/Å) is found as the most stable. However, it is about 13.5 times less stable than the most stable hydrogenated ASiNR (a_{22}). The order of structure stability for different configurations of ZSiNRs is $z_2 > z_{221} > z_{21} > z_{211} > z_{2\text{-}1} > z_1$. The possible reason is that Si atoms prefer to accept sp^3 hybridizations over sp^2 in silicene; therefore, dihydrogenation could increase the stability of the structures. In addition, similar to ASiNRs, halogenating would increase the stability of the ZSiNRs. The stability of fluorinated z_2 (− 2.064 eV/Å) is 215 times more than the hydrogenated z_2 and 0.84 less than the fluorinated a_{22}. Similar to ASiNRs, the stability of halogenated ZSiNRs decreases with increasing the atomic number of halogen atoms.

The bare pristine Klein edge is also unstable (+ 0.38 eV/Å). It is found that hydrogenated k_1 (+ 0.40 eV/Å) and k_2 (+ 0.25 eV/Å) are still unstable. However, fluorinated k_1 (− 0.65 eV/Å) and k_2 (− 1.84 eV/Å) are stabilized. Interestingly, while hydrogenated k_3 (− 0.72 eV/Å) shows metastable behavior, fluorinated k_3 (− 3.23 eV/Å) is highly stable due to the preference of sp^3 hybridization of Si edge atoms over sp^2. It is revealed that trifluorinated Klein edge (k_3) is the most stable edge structure among all edge structures of SiNRs. Furthermore, the hydrogenated k_3 can become more stable by periodically inserting a Klein vacancy terminated with two functionalization atoms k_{33} + z_2 (− 0.10 eV/Å) resulting in stabilities approaching that of hydrogenated a_{22}. It is

important to mention that the bare Klein edge can undergo a reconstruction to a pentagon-terminated Klein edge (*rk*) or to a pentagon-heptagon zigzag edge *(5-7)*, which are 0.05 and 0.03 eV/Å more stable than bare Klein edge. Although the hydrogenated $(5\text{-}7)_{11}$ is unstable (+ 0.16 eV/Å), the hydrogenated $(5\text{-}7)_{22}$ is almost stable (− 0.026 eV/Å). Interestingly enough, when the edges of *(5-7)* SiNRs are terminated with one and two fluorine atoms the formation energies are decreased to − 0.80 and − 2.07 eV/Å which are more stable than those of hydrogenated. In addition, the edge configurations of hydrogenated rk_{11} (+ 0.15 eV/Å) and rk_{21} (+ 0.81 eV/Å) are unstable. However, the hydrogenated rk_{22} is energetically more favorable with formation energy of − 0.069 eV/Å. Even more interesting is that fluorinated rk_{11} and rk_{22} are both stable with edge formation energy of – 0.798 eV/Å and – 2.104 eV/Å, respectively, emphasizing that halogenating is a decent way to increase the stability of SiNRs. Similar to $k_{33} + z_2$ structure, rk_{22} can be more stabilized by periodically inserting a Klein edge vacancy which results in a doubly hydrogenated or halogenated zigzag edge site. The hydrogenated $rk_{22} + z_2$ (− 0.083 eV/Å) is a slightly more stable than rk_{22} **(for more details see Table S3).**

Finally, the combinations of zigzag and reconstructed Klein edges are also investigated. For this reason, one edge is zigzag and the other one is reconstructed Klein. Based on the different possible edge functionalization, four types of edge functionalization are chosen as follows: a) rk_{22} - z_{22} kind, b) rk_{11} - z_{11} kind, c) rk_{22} - z_{11} kind, and d) rk_{11} - z_{22} kind.[52] The unterminated *rk* - *z* is unstable (+ 0.35 eV/Å). The edge formation energy of hydrogenated a, b, c, and d kinds are − 0.035, + 0.12, + 0.014, and + 0.009, respectively. The edge formation energy of a, b, c, and d kinds decreased to – 2.081, – 0.833, – 1.485, and – 1.428, respectively, using fluorine as the functionalization atom **(for more details see Table S4).**

Based on the calculated edge formation energies, k_3 and $k_{33} + z_2$ edges are found to be the most stable edge structures. In order to account for the experimental conditions, the edge free energies of the aftermentioned hydrogenated edge structures are calculated and plotted in **Fig. 8.** For low hydrogen chemical potential $\mu_{H2} < -2$ eV, the z_1 has minimum energy. When -2 eV $\leq \mu_{H2} < -1.4$ eV, several different edge structures have almost same amount of energy. Further increase of μ_{H2} up to – 0.2 eV, $rk_{22} + z_2$ is most favorable. For – 0.2 eV $\leq \mu_{H2} <$ + 0.5 eV, $k_{33} + z_2$ is the most stable edge structure. The edge free energy for $k_{33} + z_2$ and k_3 is almost equal for + 0.5 eV $\leq \mu_{H2} <$ + 1 eV. Finally, for $\mu_{H2} \geq$ + 1 eV, the k_3 edge structure is found as the most stable structure. For fluorine, for $\mu_{F2} < -1.9$ eV the $(5\text{-}7)_{22}$ is the most stable edge structure, while when $\mu_{F2} \geq -1.9$ eV it is k_3 **(See Fig. S1(b)).** Under ambient conditions, i.e., 300 K and 5×10^{-7} bar, the stable edges are hydrogenated $rk_{22} + z_2$ (at $\mu_{H2} = -0.694$ eV) and fluorinated k_3 (at $\mu_{F2} = -0.933$ eV).

To sum up, for ASiNRs, the a_{22} structure is the most stable structure in perfect vacuum conditions and experimentally under ambient conditions. For the hydrogenated edge SiNRs along the $<2\bar{1}\bar{1}0>$ direction, $k_{33} + z_2$ in perfect vacuum conditions and $rk_{22} + z_2$ under experimental ambient conditions are the most stable structures. Furthermore, if the edges along the $<2\bar{1}\bar{1}0>$ direction were functionalized with fluorine atoms, the k_3 structure is found as the most stable structure in both vacuum and experimental conditions.

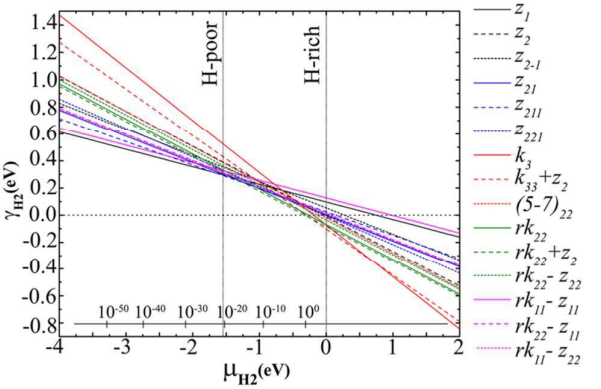

Fig. 8 Edge free energy γ_{H2} of different edge structures of hydrogenated SiNRs along $<2\bar{1}\bar{1}0>$ *versus* hydrogen chemical potential μ_{H2}, using E_{H2} as the zero reference. The allowed range for hydrogen chemical potential is indicated by vertical dotted lines. The bottom inset axis represents the pressure, in bar, of molecular H_2 corresponding to μ_{H2} when T = 300 K.

The non-spin-polarized calculations of hydrogenated z_1 show that the valence top π band meets the conduction bottom π* band at Fermi level and the bands flatten, as shown in **Fig. 9(a).** It has been found that the flat bands which cause metallicity in z_1 are induced by the p_z orbital of the outer Si atoms and are referred as to edge states. On the other hand, spin-polarized calculations of hydrogenated z_1 demonstrates that the total energies of AFM and FM states are 43.15 and 38.07 meV, lower than that of the NM state, pointing out that the AFM state is the ground state. Furthermore, the spin-up and spin-down bands are fully degenerated, and a band gap of 0.313 meV is opened at the Fermi level in AFM state, demonstrating AFM semiconducting behavior, as seen in **Fig. 9(b)**. The results are in excellent agreement with previous findings.[50,52] It should be mentioned that all halogenated z_1 structures are also AFM semiconductors.

The non-spin-polarized band structure of hydrogenated z_2 shows that it is a semiconductor with as small indirect band gap of 0.037 eV, however, the halogenated z_2 structures show metallic behavior. Considering spin-polarization, the total energy of AFM and FM states are 86.66 meV and 52.2 meV lower than that of NM state, suggesting that the AFM state is the ground state. Comparing the ΔE_{FM-AFM} of hydrogenated z_2 (34.46 meV) and hydrogenated z_1 (5.06 meV) shows that dihydrogenation enhances the stability of the AFM state. The AFM state of z_2 is also an indirect semiconductor with a band gap of 0.41 eV which is much larger than that of NM, as shown in **Fig. 9(c) and (d).** There is a good match between these results and Ref. 50.

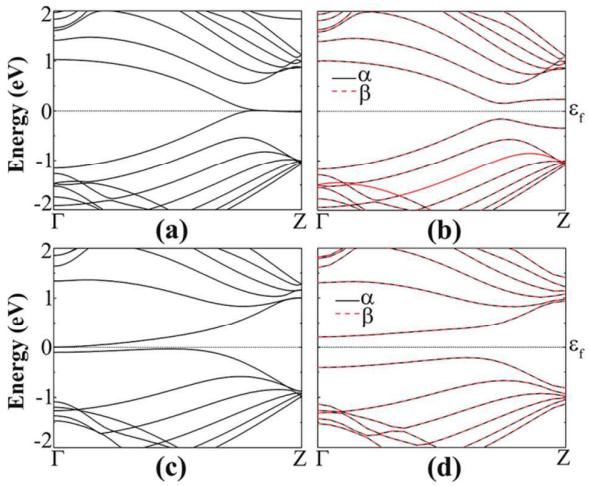

Fig. 9 Band structures of hydrogenated z_1 in the (a) NM and (b) AFM states, hydrogenated z_2 in the (c) NM and (d) AFM states.

The non-spin-polarized calculations of asymmetric hydrogenated $z_{2\text{-}1}$ indicate that there is a flat band throughout the Brillouin zone, showing a metallic behavior, as depicted in **Fig. 10(a).** Similar to zigzag edge GNRs,[45] the edge Si atoms which are attached to two hydrogen atoms have negligible contributions around Fermi level, while the adjacent atoms undertake the role of edge states, bands flattening in the range of $0 < k \leq 2\pi/3$. For the zigzag edge with mono-hydrogen termination, the p_z orbitals of the edge Si atoms have a large contribution to the Fermi level, making the bands flat in the range of $2\pi/3 < k \leq \pi$. Considering the spin-polarized calculations of hydrogenated $z_{2\text{-}1}$, it has been found that the AFM state is metallic, while becoming an indirect semiconductor (0.54 eV) with spin-up (-down) fully occupied (unoccupied) in the FM state. The hydrogenated $z_{2\text{-}1}$ shows a bipolar magnetic behavior because of fully spin-polarized states with opposite orientations around the Fermi level, as shown in **Fig. 10(b)**. The value of ΔE_{FM-AFM} for hydrogenated $z_{2\text{-}1}$ is –12.14 meV, suggesting that the FM state is the ground state. In addition, the total magnetic moment of stable FM state is 1 μB per unit cell. The results are confirmed in Refs. 50 and 51. In addition, the spin-polarized band structures of the $z_{2\text{-}1}$ functionalized with F and I show that they are FM metals, while, functionalization of $z_{2\text{-}1}$ structure with Cl or Br atom yields FM semiconducting behavior. The value of indirect band gaps for spin-up (down) channel for Cl and Br are 0.505 (0.277) eV and 0.495 (0.273) eV, respectively. Interestingly, the top valence band of spin-up touches the bottom band of spin-down at Fermi level, showing the SGS feature, as presented in **Fig. 10(d)** for Cl.

Hydrogenated z_{21} and z_{211} are direct semiconductors with band gaps of 0.175 eV and 0.160 eV, respectively. The spin-polarized calculations show that they are NM. The stable hydrogenated z_{221} structure is also a direct semiconductor with a band gap of 0.140 eV. However, the halogenated z_{221} structures have small indirect band gaps in the range of 2 - 6 meV. If spin-polarization is taken into account, the AFM state will match with the ground state, where ΔE_{FM-AFM} for hydrogenated z_{221} is equal to 48.31 meV which is more stable than that of z_1, z_2, and $z_{2\text{-}1}$ structures. Furthermore, hydrogenated z_{221} becomes an indirect semiconductor (0.285 eV) when spin-polarization is considered.

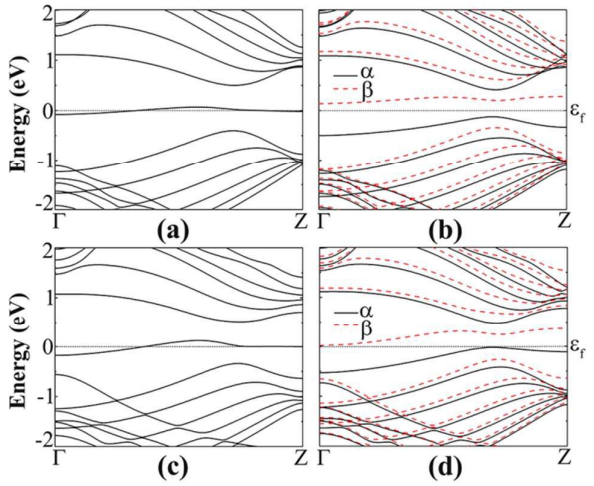

Fig. 10 Band structures of hydrogenated $z_{2\text{-}1}$ in the (a) NM and (b) FM states, chlorinated $z_{2\text{-}1}$ in the (c) NM and (d) FM states.

The unstable hydrogenated k_1 and k_2 have metallic behaviors with no sign of magnetism when spin-polarized calculations are performed. Interestingly, the stable hydrogenated k_3 is still metal **(Fig. 11(a))**, but trihydrogenation of edge Si atoms induced magnetism when spin-polarization is considered. The AFM state is the ground state (ΔE_{FM-AFM} has a small value of 4.6 meV), and a direct band gap of 0.29 eV is opened at the Fermi level, showing semiconducting behavior, as seen in **Fig. 11(b).** In addition, periodically inserting Klein vacancy in k_3, creating k_{33} + z_2, makes k_3 more stable, as mentioned before, and transforms it to a semiconductor with a band gap of 0.162 eV. Moreover, the spin-polarized calculations of hydrogenated k_{33} + z_2 show that it is not magnetic. The stable hydrogenated $(5\text{-}7)_{22}$ shows a metallic behavior without magnetism when taking into consideration spin-polarization.

The non-spin-polarized calculation of the stable hydrogenated rk_{22} shows that it is a metal (**Fig. 11(c)**), and becomes magnetic when considering polarization. The value of ΔE_{FM-AFM} is 8.8 meV, showing that the AFM state is the ground state. In addition, a band gap opening with value of 0.282 eV occurs at Fermi level, demonstrating semiconducting behavior, as shown in **Fig. 11(d)**. It should be noted that similar to hydrogenated z_2 the metallicity origin in non-spin-polarized calculations comes from the flat band located around the Fermi level. The p_z orbitals of edge Si atoms with two attached hydrogen atoms corresponds to bands which are deep in the valance bands, while the p_z orbitals of Si atoms next to edge Si atoms, the zigzag edge, ascribe to the flat bands. These flat bands give rise to magnetism in rk_{22} due to the stoner effect. The results correspond well with the literature.[52] Similar to k_3, periodically inserting dihydrogenated zigzag edge between reconstructed Klein edges, rk_{22} + z_2, cause a metal to semiconductor transformation which has a direct band gap of

0.16 eV at Γ-point. It should be mentioned that stabilizing rk_{22} *via* periodic injection of z_2 suppresses magnetism in spin-polarized calculations. The halogenated k_3, $k_{33} + z_2$, $(5\text{-}7)_{22}$, rk_{22}, and $rk_{22} + z_2$ structures shows a similar behavior as mentioned for hydrogenated structures, as seen in **Table S3.**

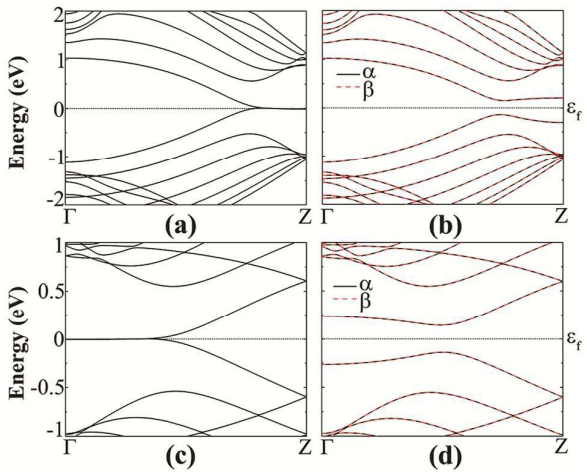

Fig. 11 Band structures of hydrogenated k_3 in the (a) NM and (b) AFM states, hydrogenated rk_{22} in the (c) NM and (d) AFM states.

The combinations of Klein and zigzag edges may result in attractive magnetic properties. The non-spin-polarized calculations of previously mentioned combinations show that they are all metallic. Taking spin-polarization into account, the hydrogenated rk_{22} - z_{11} is still an AFM semiconductor. However, different from rk_{22} *and* z_1, the band gap is spin-resolved, resulting in a band gap of 0.297 and 0.301 eV for spin-up and for spin-down, respectively. The value of ΔE_{FM-AFM} is 9.5 meV which is larger than that of rk_{22} *and* z_1. Moreover, the total magnetic moment is still 0 μB. The halogenated rk_{22} - z_{11} exhibits similar behavior as hydrogenated, as seen in **Table S4.** For spin-polarized hydrogenated rk_{11} - z_{11} and rk_{11} - z_{22} combinations, FM and AFM metallic behaviors are found in the ground state, respectively. The spin-polarized calculations of rk_{11} prove that it is not magnetic; hence it eliminates the magnetism from one edge side of the nanoribbons, as shown in **Fig. 12(c).** It means that the zigzag edge of the nanoribbons determines the total magnetic moment, as shown in **Fig. 12(a) and (b),** which is 0.92 μB for the z_{11} case and 0 μB for the z_{22} one. As discussed earlier, in z_{22} case, the atom next to the Si edge atom play the role in magnetism, the distribution of spin densities are different for two above case, causing a difference in magnetic status. For the hydrogenated rk_{22} - z_{22} case, both edges are involved in magnetism, as shown in **Fig. 12(a) and (d),** resulting in a FM ground state with total magnetic moment of 2.003 μB and ΔE_{FM-AFM} of – 22.46 meV. In addition, the whole bottom conduction band and the whole top valence bands have opposite spin orientations, showing a bipolar magnetic semiconducting behavior. The value of indirect band gap for spin-up (-down) is 0.524 (0.473) eV, see **Fig. 12(f).** Similar results are reported in Ref. 52. Functionalization with Cl and Br also give rise to FM semiconductor behavior in rk_{22} - z_{22}. Nonetheless, for the rk_{22} - z_{22} case functionalized with F and I, the results show that a weak FM metallic behavior appears in the structure.

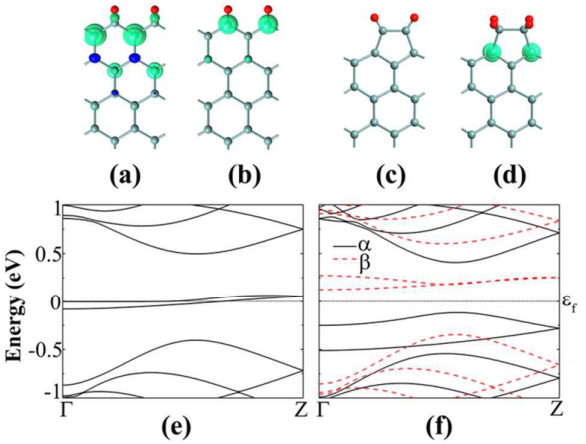

Fig. 12 Spin charge density distributions of (a) z_2, (b) z_1, (c) rk_{11} and (d) rk_{22}. The green and blue regions correspond to the isosurfaces of spin-up and spin-down channels with a spin value of 0.001 e/A^3. The band structures of hydrogenated rk_{22}-z_{22} in the (e) NM and (f) FM states

3.3 Armchair Silicene Nanoribbons doped by N or B Atoms

The electronic and magnetic properties of SiNRs can be effectively tuned by doping. In this study, the effects of doping of SiNRs with N or B impurity have been investigated. Theoretically, a single N or B doing can be substituted with Si atom in different sites of the nanoribbon. To further clarify which site is experimentally more likely to occur, the formation energy of the N or B impurity is calculated

$$E_f = E_{doped} - \left(E_{Pristine} - (m + n) E_{Si} + m E_N + n E_B \right)$$

Here, E_{doped} and $E_{Pristine}$ are the total energy of doped SiNRs with N or B impurity and the total energy of pristine SiNR, respectively. The E_{Si}, E_N, and E_B are the total energy of free Si, N, and B impurity, respectively. m and n are the number of N and B impurities in the doped SiNR, respectively. Based on the definition, the smaller value of E_f is, the more favorable the system is experimentally. **Fig. S2** shows the preferred N or B doped positions in different edge functionalized ASiNRs. has been found that the formation energy of a single substitution at the edge site is lower than other sites in the nanoribbon, indicating that the possibility of substitution of Si atoms with dopants are higher at the edges of the nanoribbons.[54-58] However, other metastable sites can be considered for practical thermodynamical conditions due to the small difference in the amount of their formation energies.[57]

The edge formation energies, band gaps, and magnetic edge states of hydrogenated and fluorinated ASiNRs doped with N or B atom are listed in **Table S5.** The formation energy of B doped ASiNRs are found to be lower than that of N-doped ASiNRs, suggesting that B impurity is easier to substitute in ASiNRs. It can also be due to the larger Pauling electronegativity (3.04) and smaller covalent radius (0.75 Å) of

the N atom compared to the B atom (Pauling electronegativity of 2.04 and covalent radius of 0.82 Å).[71] To gain better insight on the reason behind this, the bond lengths of atoms in pristine and doped of ASiNRs, for instance a_{11}, are calculated. The optimized pristine Si-Si bond length and Si-H bond length are 2.28 and 1.50 Å, respectively. In addition, the calculated Si-N bond length (1.74 Å) and N-H bond length (1.02 Å) in N-doped a_{11} are found to be shorter than Si-B bond length (1.92 Å) and B-H bond length (1.21 Å) in B doped a_{11}. It means that the values of bond length for B-doped ASiNR are more similar to values of bond length for pristine ASiNR than the N-doped ASiNR counterpart, resulting in less lattice distortion and a more stable structure.

The band structures of N- or B-doped ASiNRs show that there is a half-filled band near the Fermi level, resulting in a semiconductor-metal transition, as seen in **Fig. 13(a) and (c).** Interestingly, the band introduced by N dopant lies closer to the conduction band, while the band induced by B dopant is located near valence band. The reason behind this is that the value of ionic electronegativity of the Si atom is higher (lower) than the B (N), and hence the orbit energies of B (N) are higher (lower) than those of Si. As a result, the B (N) impurity shifts the band levels of SiNRs up (down).[55,56] It should be noted that the impurity states mostly stem from the hybridized interactions between N or B impurity and their Si atom neighbors. Besides, the spin-polarized calculations show that the N- or B-doped a_{22} and $a_{22\text{-}11}$ have null magnetic moment, which is in agreement with pristine ASiNRs.[55]

The spin-polarized calculations of hydrogenated a_{11} doped with N atom indicate that it is semiconducting in both channels with band gaps of 0.137 and 0.540 eV for spin-up and spin-down channels, respectively, see **Fig. 13(b).** However, the hydrogenated a_{11} doped with B atom is still metallic. Besides, the fluorinated a_{11} doped with N or B atom are also semiconducting. **Fig. 13(d)** shows the spin-polarized band structure of B-doped fluorinated a_{11}. Interestingly enough, the VBM of the spin-up channel touches the CBM of the spin-down channel, suggesting a semi-metallic and SGS behaviors. In other words, it shows a half-metallic behavior with 100% spin polarization current. Therefore, there is no need of energy for the electrons at the Fermi level to jump from the valence band to the conduction band.[55] The value of the band gaps for N and B case are 0.092 (0.463) eV and 0.481 (0.259) eV for spin-up (-down) channels, respectively.

Furthermore, similar to pristine hydrogenated a_{21} edge structure, spin-polarized calculations of N- or B-doped hydrogenated a_{21} shows that it behaves like a FM semiconductor. The value of band gap for spin-up (-down) electrons for N and B cases are 0.816 (0.480) eV 0.444 (0.630) eV, respectively. In addition, the values of ΔE_{FM-AFM} for N and B cases are –170.91 and –180.46 meV, respectively, which are almost twofold compare to pristine case, showing that doping increases the magnetic stability of the structure. It should be mentioned that the fluorinated a_{21} edge structure doped by N or B atoms show an AFM semiconductor behavior, as seen in **Table S5.**

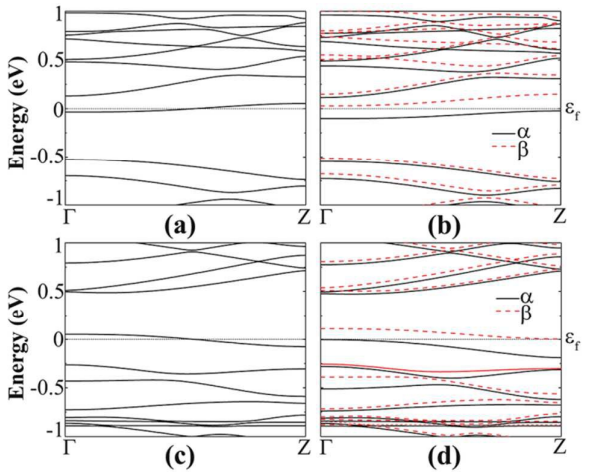

Fig. 13 Band structures of N-doped hydrogenated a_{11} in the (a) NM and (b) FM states, N-doped fluorinated a_{11} in the (c) NM and (d) FM states.

3.4 Zigzag / Klein edge Silicene Nanoribbons Doped by N or B Atom

Similar to ASiNRs, the N or B impurity prefers to be substituted for the edge Si atoms to interior ones due to the lower formation energy of edge doped SiNRs in $<2\bar{1}\bar{1}0>$ direction. The underlying reason can be attributed to the decay of edge states in ZSiNRs, as reported for GNRs.[73] **Fig. S3** indicated the preferred N or B doped positions in functionalized SiNRs along $<2\bar{1}\bar{1}0>$ direction. The non-spin-polarized calculations of doped SiNRs in the $<2\bar{1}\bar{1}0>$ direction show that they are all metallic. First, we study the effect of N or B doping on the zigzag edge SiNRs. The spin-resolved band structure of N- or B-doped hydrogenated z_1 shows that the introduction of dopants at the edge of the hydrogenated z_1 gives rise to asymmetrical spin-up and spin-down bands around E_f, suggesting that the spin degeneracy of AFM - z_1 disappeared and the mirror symmetry is broken. For the N- (B-) doped case, both spin-up and spin-down channels show semiconducting behaviors with direct band gaps of 0.161 and 0.219 eV (0.219 and 0.106 eV), respectively, as shown in **Fig. 14(a)-(d).** The origin of spin-degeneracy in pristine hydrogenated z_1 is considered to be the unpaired spin-up π band and spin-down π* band at the edge of the nanoribbons. The introduction of N or B impurity at the edge of the ZSiNR injects an additional electron or hole into the SiNR, and they would occupy the unpaired spin orbital, causing the degeneracy of bands to break. This fact that the electrons and holes tend to inject into the edge π and π* states more than interior states can be related to the local structure distortion caused by impurities at the edge of the nanoribbon.[55,56] To obtain a deeper insight into the reason of breaking degeneracy of hydrogenated z_1, the spin-density distribution of N-doped hydrogenated z_1 is plotted in **Fig. 14(e).** As can be seen, the spin-polarization at the Si edge of the SiNR which is substituted by the N impurity is fully suppressed, proving that there is no unpaired spins on the N atom. However, the spin polarization of the un-doped edge is less affected, and it is similar to the spin polarization of the pristine hydrogenated z_1. The reason

should be attributed to the less affected bond lengths of Si atoms in the un-doped edge. For both N and B cases, the total magnetic moment is 1 μB per supercell. It should be added that the fluorinated z_1 doped by N or B atoms are also semiconductors with band gap of 0.159 (0.155) eV and 0.198 (0.84) eV for spin-up (-down) channels, respectively. These results are in excellent agreement with previous studies.[54-56]

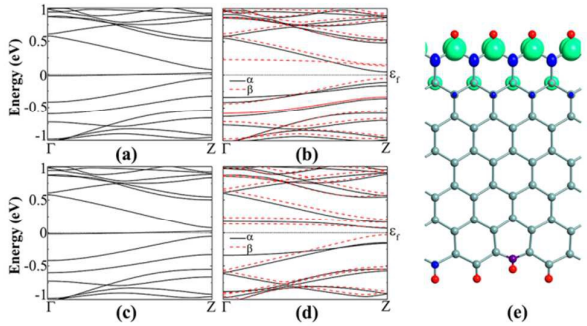

Fig. 14 Band structures of N-doped hydrogenated z_1 in the (a) NM and (b) AFM states, B-doped hydrogenated z_1 in the (c) NM and (d) FM states. (e) The spin charge density distributions of N-doped hydrogenated z_1. The purple ball represents N atom. The green and blue regions correspond to the isosurfaces of spin-up and spin-down channels with a spin value of 0.001 e/A^3.

The spin-polarized band structure of N- or B-doped z_2 shows that similar to the doped z_1, the spin degeneracy of AFM - z_2 is broken, and it becomes an AFM semiconductor with asymmetrical spin-up and spin-down bands . The value of band gaps for hydrogenated z_2 doped with N and B are 0.365 (0.352) eV and 0.444 (0.243) eV for spin-up (-down) channels, respectively. As mentioned before, there are flat bands near the Fermi level in the whole Brillouin zone for both spin-up and spin-down channels in spin-polarized band structures of asymmetric $z_{2\text{-}1}$. So that, the hydrogenated and fluorinated $z_{2\text{-}1}$ are FM direct semiconductor and FM metal, respectively. If the Fermi level shifts down to meet the top valence band, the $z_{2\text{-}1}$ would be transformed to a half-metal with the spin-down channel conducting. While, if the Fermi level shifts up to cross the bottom conduction band, the spin-up channel takes the role of conductive channel, and the spin-down channel shows an insulating behavior. One approach to moving the Fermi level up (down) is injecting electrons (holes) by n-type (p-type) doping.[51] The N- or B-doped hydrogenated $z_{2\text{-}1}$ becomes a FM indirect semiconductor with band gaps of 0.486 (0.200) eV and 0.238 (0.373) eV for spin-up (-down) channels, respectively. While, when N is doped at the edge of the fluorinated $z_{2\text{-}1}$, it is semiconducting in the spin-down channel with a direct band gap of 0.174 eV, and conducting in spin-up channel, showing a half-metallic behavior. Interestingly, when B is doped in fluorinated $z_{2\text{-}1}$, the structure keeps its FM metallic behavior, as shown in **Fig. 15.**

When N or B atom is doped in z_{221} edge structure, the AFM indirect semiconductor - z_{221} converts into a different state depending on the dopant type and functionalization atoms. The N- or B-doped hydrogenated z_{221} is still a semiconductor; however the spin-degeneracy disappears. For the N-doped, there is a direct band gap of 0.163 eV in spin-up channel, and an indirect band gap of 0.252 eV in spin-down channel. The B-doped hydrogenated z_{221} has a direct band gap of 0.372 (0.111) eV for both spin-up (-down) channel. Moreover, the fluorinated z_{221} doped with N atom is transformed into a metal. However, the B-doped fluorinated z_{221} is indirectly semiconducting (0.238 eV) in the spin-up channel, and conducting in the spin-down channel.

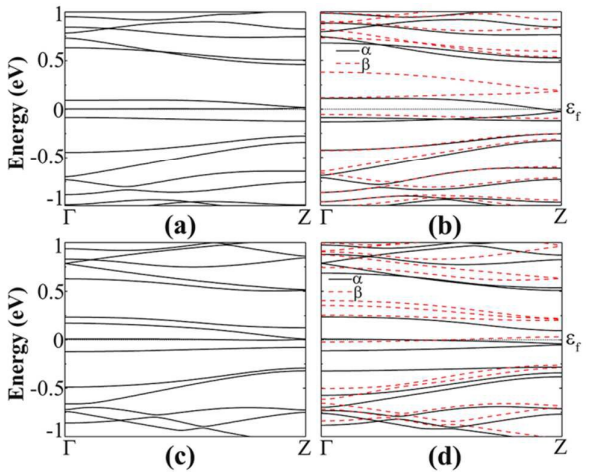

Fig. 15 Band structures of N-doped fluorinated $z_{2\text{-}1}$ in the (a) NM and (b) FM states, B-doped fluorinated $z_{2\text{-}1}$ in the (c) NM and (d) FM states.

We also address the effect of N or B doping in Klein edge SiNRs. The hydrogenated AFM direct semiconductor k_3 keeps its semiconducting character when it is doped with N or B atoms. However, doping causes the spin degeneracy to disappear. The energy band gaps for N- or B-doped hydrogenated k_3 are 0.158 (0.170) eV and 0.202 (0.089) eV for spin-up (-down) channels. The fluorinated AFM indirect semiconductor k_3 is still semiconductor when it is doped with N atom. There is a direct band gap (0.149 eV) in spin-up channel, and an indirect band gap (0.134 eV) in spin-down channel. Though, B-doped fluorinated k_3 is semiconducting (0.221 eV) in spin-up channel, it is conducting in spin-down channel. The effects of doping on AFM direct semiconductor rk_{22} are more straightforward. In both hydrogenated and fluorinated cases, the semiconducting character remains after doping, while, the spin-degeneracy of bands collapses. It is found that the doping decreases the energy band gap of hydrogenated or fluorinated rk_{22}.

Finally, we investigate the influence of the N or B doing on the magnetic properties of the combinations of zigzag and reconstructed Klein edges. The hydrogenated and fluorinated AFM direct semiconductor rk_{22} - z_{11} are transformed into FM metals when they are doped with N or B atom on the edge sites. The hydrogenated AFM metal rk_{11} - z_{22} is turned into a semiconductor with direct band gap of 0.320 eV for spin-up channel and an indirect band gap of 0.178 eV for spin-down channel when doped with a N atom, and becomes indirect semiconductor with band gap of 0.082 (0.124) eV for spin-up (-down) channel when a Si atom is replaced with a B atom. The fluorinated rk_{11} - z_{22} shows half-metallic behavior when it is

doped with N or B atom. The N-doped rk_{11} - z_{22} is semiconducting (0.178 eV) in spin-up channel, and conducting in spin-down channel. But the situation is reversed when it is doped with a B atom. The spin-up channel shows metallic behavior, while the spin-down channel is a semiconductor with a direct band gap of 0.307 eV. In FM metal rk_{11} - z_{11} case, the B atoms do not change its characteristic. However, the hydrogenated and fluorinated rk_{11} - z_{11} become semiconductors when they are doped with N atom. The N-doped hydrogenated rk_{11} - z_{11} has an indirect band gap of 0.423 (0.416) eV around its Fermi level for spin-up (-down) channel. As mentioned before, the hydrogenated rk_{22} - z_{22} is a FM indirect semiconductor. It is found that the N or B doping keeps its semiconducting behavior, while the band gap values experience a small change. The situation is a bit different for the FM metal fluorinated rk_{22} - z_{22} case. It experiences a metal to semiconductor transformation when it is doped with N atom. A direct band gap of 0.479 eV in the spin-up channel and an indirect band gap of 0.395 eV are found around its Fermi level. A half-metallic behavior is observed in the B-doped fluorinated rk_{22} - z_{22} structure. While, the spin-up channel is conducting, the spin-down channel is semiconducting with a band gap of 0.353 eV. **(For more details see Table S6 and S7).**

IV Conclusions

First-principles calculations based on DFT were used to investigate the geometry, stability, electronic and magnetic properties of different edge functionalized (–H, –F, –Cl, –Br, and –I) SiNR types, including armchair, zigzag, Klein, reconstructed Klein, reconstructed pentagon-heptagon, and their combinations. Halogenated edge SiNRs are found much more stable than those of hydrogenated edge. Although the edge stability of halogenated edge SiNRs decreases with increasing atomic number of halogen atoms, they are still more favorable than hydrogenated edge SiNRs due to their lower formation energies. Experimentally under ambient conditions, a_{22} structure along the $<1\bar{1}10>$ direction and hydrogenated rk_{22}+z_2 and fluorinated k_3 structures along the $<2\bar{1}\bar{1}0>$ direction are found as the most stable structures. It was revealed that the asymmetry in edge functionalization of two edges of ZSiNRs induce fantastic SGS and ferromagnetic metal behaviors into ZSiNRs owing to breaking of spin degeneracy of two edge states. Furthermore, the combinations of reconstructed Klein edge and zigzag edge result in various magnetic states depending on type and density of edge functional addend.

It was discovered that N or B dopant energetically tends to be substituted for the Si edge atoms, supressing the spin polarization of edge Si states. When a N or B atom is doped into fluorinated a_{11} structure, a NM semiconductor to FM SGS transition occurs. In addition, the half-metal character was also found in fluorinated $z_{2\text{-}1}$ and k_3 when they are doped with N and B atoms, respectively. It was also observed that several peculiar magnetic states, such as ferromagnetic metal, AFM metal, half-metal, and SGS, can be obtained in the combinations of reconstructed Klein edge and zigzag edge depending of dopant atom and edge functional atom and its density. These predicted properties of SiNRs will have potential applications in advancement of nanoelectronics and spintronics.

Acknowledgements

This work was supported in part by the Florida Education Fund's McKnight Junior Faculty Fellowship.

References

1 K. S. Novoselov, A. K. Geim, S. Morozov, D. Jiang, Y. Zhang, S. Dubonos, I. Grigorieva, and A. Firsov, *Science*, 2004, **306**, 666-669.
2 K. Novoselov, A. K. Geim, S. Morozov, D. Jiang, M. Katsnelson, I. Grigorieva, S. Dubonos, and A. Firsov, *Nature*, 2005, **438**, 197-200.
3 A. Kara, H. Enriquez, A. Seitsonen, L. C. Lew Yan Voon, S. Vizzini, and H. Oughaddou, *Surf. Sci. Rep.*, 2012, **67**, 1-18.
4 S. Z. Butler, S. M. Hollen, L. Cao, Y. Cui, J. A. Gupta, H. R. Gutiérrez, T. F. Heinz, S. S. Hong, J. Huang, A. F. Ismach *et al*., *ACS Nano*, 2013, **7**, 2898-2926.
5 M. Xu, T. Liang, M. Shi, H. Chen, *Chem. Rev.,* 2013*,* **113**, 3766-379.
6 M. Houssa, A. Dimoulas and A. Molle, *J. Phys. Condens. Matter.,* 2015, **27**, 253002
7 L. Tao, E. Cinquanta, D. Chiappe, C. Grazianetti, M. Fanciulli, M. Dubey, A. Molle, and D. Akinwande, *Nat. Nanotechnol.*, 2015, **10**, 227-231.
8 K. Takeda and K. Shiraishi, *Phys. Rev. B*, 1994, **50**, 14916.
9 G. G. Guzmán-Verri and L. L. Y. Voon, *Phys. Rev. B*, **2007**, 76, 075131.
10 P. Vogt, P. De Padova, C. Quaresima, J. Avila, E. Frantzeskakis, M. C. Asensio, A. Resta, B. Ealet, and G. Le Lay, *Phys. Rev. Lett*., 2012, **108**, 155501.
11 B. Feng, Z. Ding, S. Meng, Y. Yao, X. He, P. Cheng, L. Chen, and K. Wu, *Nano Lett.,* 2012, **12**, 3507–3511.
12 J. Mannix, B. Kiraly, B. L. Fisher, M. C. Hersam, and N. P. Guisinger, *ACS Nano*, 2014, **8**, 7538-7547.
13 L. Meng, Y. Wang, L. Zhang, S. Du, R. Wu, L. Li, Y. Zhang, G. Li, H. Zhou, W. A. Hofer *et al*., *Nano Lett.*, 2013, **13**, 685-690.
14 A. Fleurence, R. Friedlein, T. Ozaki, H. Kawai, Y. Wang, and Y. Yamada- Takamura, *Phys. Rev. Lett.* 2012, **108**, 245501.
15 T. Aizawa, S. Suehara, and S. Otani, *J. Phys. Chem. C*, 2014, **118**, 23049-23057.
16 S. Lebègue and O. Eriksson, *Phys. Rev. B*, 2009, **79**, 115409.
17 H. Şahin, S. Cahangirov, M. Topsakal, E. Bekaroglu, E. Akturk, R. T. Senger, and S. Ciraci, *Phys. Rev. B,* 2009, **80**, 155453.
18 L. Chen, C. C. Liu, B. Feng, X. He, P. Cheng, Z. Ding, S. Meng, Y. Yao and K. Wu, *Phys. Rev. Lett.,* 2012, **109**, 056804.
19 S. Cahangirov, M. Topsakal, E. Aktürk, H. Şahin and S. Ciraci, *Phys. Rev. Lett*., 2009, **102**, 236804.
20 M. Ezawa, *Phys. Rev. Lett*., 2012, **109**, 055502.
21 A. Dyrdal and J. Barnas, *Phys. Status Solidi PRL*, 2012, 6, 340-342.
22 C.C. Liu, W.X. Feng, and Y.G. Yao, *Phys. Rev. Lett.*, 2011, **107**, 076802.
23 T. P. Kaloni, M. Tahir, and U. Schwingenschlogl, *Sci. Rep*. 2013, **3**, 3192.
24 H. Liu, J. Gao, and J. Zhao, *J. Phys. Chem. C*, 2013, 117, 10353.
25 Y. Ding and Y. Wang, *Appl. Phys. Lett*., 2013, **103**, 043114.
26 Y. Cai, C.-P. Chuu, C. M. Wei, and M. Y. Chou, *Phys. Rev. B*, 2013, **88**, 245408.

27 B. Aufray, A. Kara, S. Vizzini, H. Oughaddou, C. Leandri, B. Ealet, and G. Le Lay, *Appl. Phys. Lett.,* 2010, **96**, 183102.
28 P. De Padova, C. Quaresima, C. Ottaviani, P. M. Sheverdyaeva, P. Moras, C. Carbone, D. Topwal, B. Olivieri, A. Kara, H. Oughaddou, B. Aufray, G. Le Lay *et al.*, *Appl. Phys. Lett.,* 2010, **96**, 261905.
29 P. De Padova, O. Kubo, B. Olivieri, C. Quaresima, T. Nakayama, M. Aono, and G. Le Lay, *Nano Lett.,* 2012, **12**, 5500-5503.
30 M. R. Tchalala, H. Enriquez, A. J. Mayne, A. Kara, S. Roth, M. G. Silly, A. Bendounan, F. Sirotti, T. Greber, B. Aufray *et al.*, *Appl. Phys. Lett.* ,2013, **102**, 083107.
31 P. Wagner, V. V. Ivanovskaya, M. Melle-Franco, B. Humbert, J. -J. Adjizian, P. R. Briddon, C. P. Ewels, *Phys. Rev. B*, 2013, **88**, 094106.
32 Y. L. Song, Y. Zhang, J.M. Zhang, D. B. Lu and K.W. Xu, *Eur. Phys. J. B,* 2011, **79**, 197.
33 M. E.Dávila, A. Marele, P. De Padova, I. Montero, F. Hennies, A. Pietzsch, M. N. Shariati, J. M. Gómez-Rodríguez and G. Le Lay, *Nanotechnology*, 2012, **23**, 385703.
34 Y. Liang, V. Wang, H. Mizuseki and Y. Kawazoe, *J. Phys.: Condens. Matter,* 2012, **24**, 455302.
35 C. Xu, G. Luo, Q. Liu, J. Zheng, Z. Zhang, S. Nagase, Z. Gao, and J. Lu, 2012, *Nanoscale* **4**, 3111.
36 S. M. Aghaei and I. Calizo, *J. App. Phys.,* 2015, **118**, 104304.
37 H. Dong, D. Fang, B. Gong, Y. Zhang, E. Zhang and S. Zhang, *J. Appl. Phys.,* 2015, **117** 064307.
38 Q. G. Jiang, J. F. Zhang, Z. M. Ao and Y. P. Wu, J. *Mater. Chem. C,* 2015, **3**, 3954-3959.
39 S. M. Aghaei and I. Calizo, *SoutheastCon 2015*, 2015, 1-6.
40 M. Kan, J. Zhou, Y. Li, and Q. Sun, *Appl. Phys. Lett.,*2012, **100**, 173106.
41 M. Kan, J. Zhou, Q. Sun, Q. Wang, Y. Kawazoe, and P. Jena, *Phys. Rev. B,* **2012***,* 85, 155450.
42 T. Wassmann, A. P. Seitsonen, A. M. Saitta, M. Lazzeri and F. Mauri, *Phys. Rev. Lett.*, 2008, **101**, 096402.
43 G. Lee and K. Cho*, Phys. Rev. B*, 2009, **79**, 165440.
44 K. A. Ritter and J. W. Lyding, *Nat. Mater.,* 2009, **8**, 235.
45 S. Bhandary, O. Eriksson, B. Sanyal and M. I. Katsnelson, *Phys. Rev. B*, 2010, **82**, 165405.
46 J. Kunstmann, C. Özdoğan, A. Quandt, and H. Fehske, *Phys. Rev. B*, 2011, **83**, 045414.
47 P. Wagner, C. P. Ewels, V. V. Ivanovskaya, P. R. Briddon, A. Pateau, B. Humbert, *Phys. Rev. B,* 2011, **84**, 134110.
48 X. H. Zheng, X. L. Wang, L. F. Huang, H. Hao, J. Lan and Z. Zeng, *Phys. Rev. B*, 2012, **86**, 081408.
49 P. Wagner, C. P. Ewels, J.-J. Adjizian, L. Magaud, P. Pochet, S. Roche, A. Lopez- Bezanilla, V. V. Ivanovskaya, A. Yaya, M. Rayson, *et al*, *J. Phys. Chem. C*, 2013, **117**, 26790-26796.
50 D. Fang, S. Zhang, and H. Xu, *RSC Adv.,* 2013, **3**, 24075.
51 Y. Ding and Y. Wang, *Appl. Phys. Lett.,* 2013, **102**, 143115.
52 Y. Ding and Y. Wang, *Appl. Phys. Lett.,* 2014, **104**, 083111.
53 X. F. Yang, Y. S. Liu, J. F. Feng, X. F. Wang, C. W. Zhang and F. Chi, *J. Appl. Phys*., 2014, **116**, 124312.
54 F. B. Zheng, C. W. Zhang, P. J. Wang, S. S. Li, *J. Appl. Phys.*, 2013, **113**, 154302.
55 F. B. Zheng, C. W. Zhang, S. S. Yan, F. Li, *J. Mater. Chem. C*, 2013, **1**, 2735.
56 H. X. Luan, C. W. Zhang, F. B. Zheng, P. J. Wang, *J. Phys. Chem. C*, 2013, **117**, 13620-13626.
57 J.-M. Zhang, W.-T. Song, K.-W. Xu and V. Ji, *Comput. Mater. Sci.*, 2014, **95**, 429.
58 L. Ma, J. M. Zhang, K. W. Xu, V. Ji, *Physica E*, 2014, **60**, 112-117.
59 K. Zberecki, R. Swirkowicz, J. Barnaś, *Phys. Rev. B*, 2014, **89**, 165419.
60 A. Lherbier, X. Blase, Y. M. Niquet, F. Triozon, S. Roche, *Phys. Rev. Lett.* 2008, **101**, 036808.
61 M. Brandbyge, J.-L. Mozos, P. Ordej_on, J. Taylor, and K. Stokbro, *Phys. Rev. B*, 2002, **65**, 165401.
62 J. Taylor, H. Guo, and J. Wang, *Phys. Rev. B,* 2001*,* **63**, 245407.
63 Atomistix Toolkit version 2015.0; QuantumWise, Copenhagen, Denmark; see **http://www.quantumwise.com/**
64 K. Reuter and M. Scheffler, *Phys. Rev. B*, 2002, **65**, 035406.
65 G. Soldano, F. Juarez, B. Teo and E. Santos, *Carbon*, 2014, **78**, 181.
66 D.R. Stull and H. Prophet, JANAF Thermochemical Tables, 2nd ed. U.S. National Bureau of Standards, Washington, DC, 1971.
67 Y.-W. Son, M. L. Cohen, and S. G. Louie, *Phys. Rev. Lett*., 2006, **97**, 216803.
68 S. Cahangirov, M. Topsakal, and S. Ciraci, *Phys. Rev. B*, 2010, **81**, 195120.
69 X. H. Zheng, L. F. Huang, X. L. Wang, J. Lan, and Z. Zeng, *Comput. Mater. Sci.*, 2012, **62**, 93-98.
70 G. G. Guzman-Verri and L. C. L. Y. Voon, *J. Phys.: Condens. Matter*, 2011, **23**, 145502-145506.
71 **http://www.webelements.com/**
72 N. Gao, W. T. Zheng and Q. Jiang, *Phys. Chem. Chem. Phys.*, 2012, **14**, 257-261.
73 S. Dutta and S. K. Pati, *J. Phys. Chem. B*, 2008, **112**, 1333-1335.

Edge Functionalization and Doping Effects on Stability, Electronic and Magnetic Properties of Silicene Nanoribbons

S. M. Aghaei,[a] M. M. Monshi,[a] I. Torres,[a] and I. Calizo[a,b]

Table of Contents Entry

A spectacular SGS character with 100% spin polarized currents around the Fermi level is found in $Z_{2\text{-}1}$ functionalized with Cl.